



HAL
open science

Numerical modeling and experimental characterization of the AC conductivity and dielectric properties of CNT/polymer nanocomposites

Xiaoxin Lu, Anne Zhang, Olivier Dubrunfaut, Delong He, Lionel Pichon,
Jinbo Bai

► **To cite this version:**

Xiaoxin Lu, Anne Zhang, Olivier Dubrunfaut, Delong He, Lionel Pichon, et al.. Numerical modeling and experimental characterization of the AC conductivity and dielectric properties of CNT/polymer nanocomposites. *Composites Science and Technology*, 2020, 194, pp.108150. 10.1016/j.compscitech.2020.108150 . hal-02546459

HAL Id: hal-02546459

<https://hal.science/hal-02546459>

Submitted on 1 Jun 2020

HAL is a multi-disciplinary open access archive for the deposit and dissemination of scientific research documents, whether they are published or not. The documents may come from teaching and research institutions in France or abroad, or from public or private research centers.

L'archive ouverte pluridisciplinaire **HAL**, est destinée au dépôt et à la diffusion de documents scientifiques de niveau recherche, publiés ou non, émanant des établissements d'enseignement et de recherche français ou étrangers, des laboratoires publics ou privés.

Numerical modeling and experimental characterization of the AC conductivity and dielectric properties of CNT/polymer nanocomposites

Xiaoxin Lu^{a,*}, Anne Zhang^b, Olivier Dubrunfaut^a, Delong He^b, Lionel Pichon^a, Jinbo Bai^b

^a*Université Paris-Saclay, CentraleSupélec, CNRS, Laboratoire de Génie Électrique et Électronique de Paris, 91192, Gif-sur-Yvette, France.*
Sorbonne Université, CNRS, Laboratoire de Génie Électrique et Électronique de Paris, 75252, Paris, France.

^b*Université Paris-Saclay, CentraleSupélec, CNRS, Laboratoire Mécanique des Sols, Structures et Matériaux, 91190, Gif-sur-Yvette, France.*

Abstract

In this work, we proposed a multiscale numerical model to estimate the electric conductivity and dielectric constants of the CNT/polymer nanocomposites, taking into account the tunneling effect between neighbouring CNTs separated at nanoscale and the frequency-dependent dielectric properties of each components. Finite element method was employed to solve the formulations, and the CNTs were modeled by highly conductive line segments in order to avoid the mesh problems. Experiments have been carried out in carbon nanotubes/epoxy nanocomposites in order to compare to the simulation results. The numerical estimations of the electric conductivity are in good agreement with the experimental measurement by network analyzers. Moreover, the calculated dielectric permittivity agrees with the experimental data for the nanocomposites whose CNT content is beyond percolation threshold. Below percolation threshold, the proposed model also works well in the prediction of dielectric constants when the frequency is over 10^3 Hz.

Keywords:

A. Nano composites; A. Carbon nanotubes; B. Dielectric constants; B. Electric properties; C. Finite element analysis (FEA).

*Corresponding author *Email: xiaoxin.lu@geeps.centralesupelec.fr*

1. Introduction

The unique properties of carbon nanotube (CNT), *i.e.*, high aspect ratio, low molecular weight, superior thermal, mechanical and electrical properties, have attracted increasing interest of scientists since it was first reported in 1991 [1]. Dispersing CNTs into polymeric materials as nanoscale fillers can strongly enhance their mechanical, thermal and electrical properties, showing significant potential in multifunctional devices [2]. Since last decade, the dielectric properties of CNT/polymer nanocomposites have been investigated, pursuing high dielectric constant combined with flexibility and lightweight, which can be used in a variety of applications such as electromagnetic interference (EMI) shielding material, high-charge storage capacitors and aerospace devices [3–7].

There have been numerous experimental studies on the dielectric properties of the CNT/polymer nanocomposites, preparing the dielectrics with high dielectric permittivity [8–13]. Furthermore, focusing on the charge storage application, efforts have been done to develop the CNT-reinforced nanocomposites with both high dielectric permittivity and low dielectric loss. For instance, Begum et al. [14] employed the solution casting method to fabricate the PVDF/functionalized multi-walled carbon nanotubes (MWCNTs) with enhanced dielectric permittivity but low dielectric loss due to the strong interfacial interaction between MWCNTs and PVDF. Chang et al. [15] prepared the MWCNT/epoxy composites using microwave curing and thermal curing respectively, finding that the former fabrication method leads to better dielectric properties than the latter one attributed to a better distribution of CNTs. Besides, Zhang et al. [16] developed an expanded graphite-MWCNT/cyanate ester ternary composite, and Ameli et al. [17] reported nano/microcellularpolypropylene/CNT nanocomposites by melt compounding in which the cellular structure was introduced by foaming. Both of the composite systems exhibit high dielectric permittivity and low dielectric loss successfully.

The experimental results demonstrate that the percolation threshold and dielectric properties are dependent on the type, aspect ratio and dispersion of CNTs [15, 18], as well as the interaction between CNT and polymer matrix [14]. However, it is difficult to clearly differentiate between the effects of the above factors by experimental techniques. It is thus valuable to de-

velop the models for the predictions of the electric and dielectric properties of the CNT/polymer nanocomposites. Analytical models based on effective medium theory can be used to predict the composite permittivity [19]. For example, Maxwell-Garnett model [20, 21] has been employed to describe the effective permittivity of the polymer composites with conductive fillers characterized by high aspect ratio, which have taken into account the volume fraction and shape of the fillers. However, the results are only accurate at the filler concentration before percolation threshold, and the tunneling effect is neglected which plays dominant role in the electric properties of the nanocomposites. Although the tunneling effect has been well considered in the simulation of statistic electric properties under DC conduction [22, 23], its significance on dielectric properties and AC conductivities of nanocomposites has not been researched by numerical modeling. Recently, Xia et al. [24] developed a new effective-medium theory considering all the interface effects, which works well at low frequency but becomes blurred at high frequency. Continuum models including finite element analysis [25–28] have been reported for studying the dielectric constants of the composites, but few work has been done for the nanocomposite with conductive fillers of extremely high aspect ratio (> 100).

In this work, we proposed a numerical model to investigate the AC conductivity and the frequency-dependent dielectric constants of CNT/polymer nanocomposites, which is solved by the finite element method. The tunneling effect between neighbouring CNTs separated at nanoscale has been incorporated within the model, and the dielectric constants of the components was considered to be frequency-dependent. The effective conductivity and dielectric constants have been evaluated numerically by appropriate definitions of effective quantities through homogenization. To validate this model, we have prepared the CNT/epoxy nanocomposite samples with various CNT contents, and the CNTs are randomly dispersed in the matrix. The AC conductivity and dielectric permittivity of the samples were measured and compared with the numerical estimations. The effects of CNT aspect ratio on the electric and dielectric properties were further discussed.

2. Numerical model of the dielectric properties of CNT/polymer composites

In this work, the microstructure of the CNT/polymer composites as shown in Fig. 1 (a) is generated by Random sequential addition (RSA)

algorithm [29], which ensures that the CNT fillers are randomly distributed without overlapping. The side length of the representative volume element (RVE) is L , and the periodical boundary condition is employed to form an infinite composite material. The CNTs are assumed to be straight whose length is l , and diameter is D . The aspect ratio is defined as $\eta = l/D$. As shown in Fig. 1 (b), the position and orientation of CNTs are determined by the head point coordinate \mathbf{x}^0 and two orientation parameters in spherical coordinates, polar angle θ and azimuthal angle φ , respectively. All the parameters are generated following uniform distribution by a pseudorandom number generator in order to obtain a random and isotropic distribution of CNTs [30].

$$\mathbf{x}_i^0 = L \times (\text{rand}, \text{rand}, \text{rand}), \quad (1)$$

$$\varphi_i = 2\pi \times \text{rand} \quad (2)$$

$$\theta_i = \cos^{-1}(\text{rand}). \quad (3)$$

where i is the index of i th CNT and ‘rand’ denotes uniformly generated random number in the interval $[0, 1]$. It should be noted that by applying periodical boundary condition, the CNT will be separated to several segments and the external parts will be relocated to the RVE when it penetrates the boundary planes.

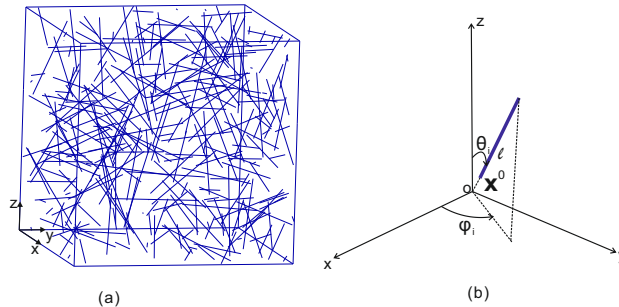


Figure 1: (a) RVE model of the CNT/polymer nanocomposite with 200 CNT fillers. (b) i th CNT in space.

The configuration and the meshes are generated by GMSH [31], and the finite element analysis is performed by programming using Matlab. We consider a RVE defined in a domain Ω , which contains N straight CNTs randomly distributed in the polymer matrix, associated to Γ_n ($n = 1, 2, \dots, N$). The

conduction mechanism according to tunneling effect is introduced between the neighbouring CNTs when their shortest distance is at nanoscale.

In the dielectric matter, the relation between the electric displacement \mathbf{D} and the electric field \mathbf{E} is given by

$$\mathbf{D} = \varepsilon_0 \boldsymbol{\varepsilon} \mathbf{E}, \quad (4)$$

where $\boldsymbol{\varepsilon}$ is the relative permittivity of the material and $\varepsilon_0 \approx 8.85 \times 10^{-12}$ F/m denotes the permittivity of free space.

According to the Maxwell equations, we have

$$\nabla \cdot \mathbf{D} = \rho, \quad (5)$$

where ρ is the volumetric charge density, $\nabla \cdot$ denotes the divergence operator.

Combing Eq. (5) with the continuity equation

$$\nabla \cdot \mathbf{J} = -\partial \rho / \partial t, \quad (6)$$

and Ohm's law

$$\mathbf{J} = \boldsymbol{\sigma} \mathbf{E}, \quad (7)$$

we obtain

$$\nabla \cdot (\boldsymbol{\sigma} + i\omega \varepsilon_0 \boldsymbol{\varepsilon}) \mathbf{E} = \mathbf{0}, \quad (8)$$

in case of sinusoidal \mathbf{E} of angular frequency ω . $\boldsymbol{\sigma}$ denotes the electric conductivity and \mathbf{J} is the electric current density.

Therefore, for the dielectric material, the current density induced by the electric field is given by

$$\mathbf{J}^d = (\boldsymbol{\sigma} + i\omega \varepsilon_0 \boldsymbol{\varepsilon}) \mathbf{E}. \quad (9)$$

In the case of alternating current, the total electromagnetic power within the domain Ω , \overline{W} for this model, including the contribution of both polymer matrix and CNTs, is defined by

$$\overline{W} = \frac{1}{2} \left(\int_{\Omega} \omega_m(\mathbf{x}) d\Omega + \int_{\Gamma} \omega_c(\mathbf{x}) d\Gamma \right), \quad (10)$$

where Γ denotes collectively the lines associated with CNTs and the density functions of polymer matrix (ω_m) and CNTs (ω_c), are expressed by

$$\omega_m(\mathbf{x}) = \mathbf{J}^d(\mathbf{x}) \cdot \mathbf{E}(\mathbf{x}), \quad \omega_c(\mathbf{x}) = \mathbf{J}_c^d(\mathbf{x}) \cdot \mathbf{E}_c(\mathbf{x}). \quad (11)$$

Here, the electric field \mathbf{E} and the line electric field on CNT \mathbf{E}^c are defined by $\mathbf{E}(\mathbf{x}) = -\nabla\phi(\mathbf{x})$ and $\mathbf{E}_c = -\nabla_{\Gamma}\phi$, where $\phi(\mathbf{x})$ is the electric potential.

The nonlinear tunneling effect conduction has been described in details in [32], and has been introduced to several works concerning the electric properties of nanocomposites [33, 34]. Considering the tunneling effect in the extremely thin polymer film between the neighbouring CNTs, the current density in the matrix $\mathbf{j}(\mathbf{x})$ satisfies:

$$\mathbf{J}^d = \begin{cases} (\boldsymbol{\sigma}_m + i\omega\epsilon_0\boldsymbol{\epsilon}_m(\omega))\mathbf{E} & \text{if } d(\mathbf{x}) \geq d_{cutoff}, \\ \mathcal{G}(\mathbf{E}, d)\frac{\mathbf{E}}{|\mathbf{E}|} + i\omega\epsilon_0\boldsymbol{\epsilon}_t\mathbf{E} & \text{if } d(\mathbf{x}) < d_{cutoff}, \end{cases} \quad (12)$$

where $\boldsymbol{\sigma}_m$ and $\boldsymbol{\epsilon}_m(\omega)$ are the electric conductivity tensor and the relative permittivity tensor of the polymer matrix when neglecting tunneling effect, d_{cutoff} is a cut-off distance above which the tunneling effect can be neglected, and \mathcal{G} is the tunneling current defined by [35]

$$\begin{aligned} \mathcal{G}(\mathbf{E}, d) &= \frac{2.2e^3 |\mathbf{E}|^2}{8\pi h\Phi_0} \exp\left(-\frac{8\pi}{2.96he|\mathbf{E}|}(2m)^{\frac{1}{2}}\Phi_0^{\frac{3}{2}}\right) \\ &+ \left[3 \cdot \frac{(2m\Phi_0)^{\frac{1}{2}}}{2}\right](e/h)^2 |\mathbf{E}| \exp\left[-\left(\frac{4\pi d}{h}\right)(2m\Phi_0)^{\frac{1}{2}}\right]. \end{aligned} \quad (13)$$

Φ_0 is the energy barrier height that the electrons cross, d is the distance between a pair of CNTs, and h , e and m denote Plank's constant, the charge of an electron and a material parameter. It should be noted that the separation between pair of CNTs, $d(\mathbf{x})$, should always be larger than the van der Waals separation distance d_{vdW} according to the Pauli exclusion principle[36, 37].

The local regions in the polymer matrix turn to be conductive according to tunneling effect when $d(\mathbf{x}) < d_{cutoff}$, leading to the local relative permittivity $\boldsymbol{\epsilon}_t$, such as

$$\boldsymbol{\epsilon}_t = \boldsymbol{\epsilon}'_t(\omega) - i\frac{\boldsymbol{\sigma}_t}{\omega\epsilon_0}, \quad (14)$$

Here

$$\boldsymbol{\sigma}_t = \mathcal{G}'(\|\mathbf{E}\|) \cdot \frac{\mathbf{E} \otimes \mathbf{E}}{\|\mathbf{E}\|^2} + \mathcal{G}(\|\mathbf{E}\|) \cdot \frac{\|\mathbf{E}\|^2\mathbf{I} - \mathbf{E} \otimes \mathbf{E}}{\|\mathbf{E}\|^3} \quad (15)$$

where \mathbf{I} denotes the second-order identity tensor, and $\mathcal{G}'(\|\mathbf{E}\|)$ is expressed by:

$$\mathcal{G}'(\|\mathbf{E}\|) = 2A\|\mathbf{E}\| \exp\left(-\frac{B}{\|\mathbf{E}\|}\right) + AB \exp\left(-\frac{B}{\|\mathbf{E}\|}\right) + C, \quad (16)$$

with

$$A = \frac{2.2e^3}{8\pi h\Phi_0}, \quad B = \frac{8\pi}{2.96he}(2m)^{\frac{1}{2}}\Phi_0^{\frac{3}{2}}, \quad (17)$$

and

$$C = 3 \cdot \frac{(2m\Phi_0)^{\frac{1}{2}}}{2}(e/h)^2 \exp[-(\frac{4\pi d}{h})(2m\Phi_0)^{\frac{1}{2}}]. \quad (18)$$

CNTs can be regarded as cylinders with tiny diameter D , resulting in a significantly large aspect ratio which can be as high as 10^3 . Thus, it is cumbersome to mesh them along their diameter directions which can create large amount of meshes beyond the computational ability. To overcome this limitation, we replace the CNTs with finite diameter by highly conducting lines. The local constitutive relationships relating the line current density \mathbf{j}^c with line electric field \mathbf{E}^c in the CNTs is defined by

$$\mathbf{J}_c^d(\mathbf{x}) = (\boldsymbol{\sigma}_c + i\omega\epsilon_0\boldsymbol{\epsilon}_c)\mathbf{E}_c, \quad (19)$$

where $\boldsymbol{\sigma}_c$ and $\boldsymbol{\epsilon}_c$ denote the equivalent line electric conductivity and equivalent line relative permittivity of CNT, respectively, which are dependent on the diameter D through:

$$\boldsymbol{\sigma}_c = \frac{\pi D^2}{4}\sigma_c^0\mathbf{n} \otimes \mathbf{n}, \quad (20)$$

and

$$\boldsymbol{\epsilon}_c = \frac{\pi D^2}{4}\epsilon_c^0\mathbf{n} \otimes \mathbf{n}. \quad (21)$$

In above, \mathbf{n} is the unit direction vector of CNT (see in Fig. 1 (b)), σ_c^0 and ϵ_c^0 denote electric conductivity and relative permittivity of the CNT along \mathbf{n} direction (see [38–40] for more details). As a conductive filler, the relative permittivity of the CNTs obeys

$$\epsilon_c^0 = (\epsilon_c^0)' - i\frac{\sigma_c^0}{\omega\epsilon_0}. \quad (22)$$

Minimizing (10) with respect to the displacement field, and using Eqs. (11)-(12), we obtain the weak form which can be solved by the finite element method:

$$\int_{\Omega} \mathbf{J}_d(\phi) \cdot \nabla(\delta\phi)d\Omega - \int_{\Gamma} \nabla_{\Gamma}\phi \cdot (\boldsymbol{\sigma}^c + i\omega\epsilon_0\boldsymbol{\epsilon}^c)\nabla_{\Gamma}(\delta\phi)d\Gamma = 0, \quad (23)$$

where $\delta\phi \in H^1(\Omega)$, $\delta\phi = 0$ over $\partial\Omega$, and $\phi \in H^1(\Omega)$, ϕ satisfying the periodic boundary conditions over $\partial\Omega$

$$\phi(\mathbf{x}) = -\bar{\mathbf{E}} \cdot \mathbf{x} + \tilde{\phi}(\mathbf{x}) \quad \text{on } \partial\Omega \quad (24)$$

and where $\tilde{\phi}(\mathbf{x})$ is a periodic function over Ω , such as $\langle \tilde{\phi}(\mathbf{x}) \rangle = 0$.

The effective electric conductivity tensor $\bar{\boldsymbol{\sigma}}$ is defined as:

$$\bar{\boldsymbol{\sigma}}(\bar{\mathbf{E}}) = \bar{\boldsymbol{\sigma}}' + i\bar{\boldsymbol{\sigma}}'' = \frac{\partial \bar{\mathbf{J}}^d(\bar{\mathbf{E}})}{\partial \bar{\mathbf{E}}}, \quad (25)$$

where $\bar{\mathbf{J}}^d$ is the effective current density expressed by:

$$\bar{\mathbf{J}}^d = \frac{1}{V} \left(\int_{\Omega} \mathbf{J}^d(\mathbf{x}) d\Omega + \int_{\Gamma} \mathbf{J}_c^d(\mathbf{x}) d\Gamma \right), \quad (26)$$

and $\bar{\mathbf{E}}$ is the effective electric field given by:

$$\bar{\mathbf{E}} = \frac{1}{V} \int_{\Omega} \mathbf{E}(\mathbf{x}) d\Omega, \quad (27)$$

where V is the volume of Ω .

The real part of the effective conductivity in Eq. (25), $\bar{\boldsymbol{\sigma}}'$, corresponds to the AC conductivity measured by the experimental techniques.

Moreover, the effective dielectric loss, $\bar{\boldsymbol{\epsilon}}''$, is estimated by

$$\bar{\boldsymbol{\epsilon}}(\bar{\mathbf{E}}) = \bar{\boldsymbol{\epsilon}}' - i\bar{\boldsymbol{\epsilon}}'' = \frac{1}{\epsilon_0} \frac{\partial \bar{\mathbf{D}}(\bar{\mathbf{E}})}{\partial \bar{\mathbf{E}}}, \quad (28)$$

where

$$\bar{\mathbf{D}} = \frac{1}{V} \left(\int_{\Omega} \mathbf{D}(\mathbf{x}) d\Omega + \int_{\Gamma} \mathbf{D}_c(\mathbf{x}) d\Gamma \right) \quad (29)$$

and $\mathbf{D}_c(\mathbf{x}) = \boldsymbol{\epsilon}_c(\mathbf{x})\mathbf{E}_c(\mathbf{x})$.

3. Experiment procedure

3.1. Materials and preparation of CNT/epoxy nanocomposites

Multi-wall CNTs were acquired from Nanocyl (NC7000). The nanotubes average size is 9.5 nm in outer diameter and 1.5 μm in length, which corresponds to an aspect ratio of 158. The epoxy resin used as polymer matrix is composed of a resin (1080S, Resoltech) and a hardener (1084, Resoltech)

mixed in a 100:33 weight ratio. Neat epoxy and 6 composites samples were fabricated with different CNT weight fractions ranging from 0.05 wt% to 1 wt%, corresponding to 0.03 vol% to 0.50 vol%, respectively. Neat epoxy were fabricated by manually mixing 1080S and 1084 components in the aforementioned weight ratio. To fabricate the CNTs/Epoxy nanocomposites, the desired weights of CNT were added to the 1080S resin and dispersed using a three-roll mill (EXAKT), following a pre-optimised procedure [41]. After adding the hardener, the mixtures were poured into a mold and shaped under a hot press for 2 hours at 60°C under 7 bars, followed by a 15-hour long curing at 60°C under atmospheric pressure. The final samples were 7 mm in diameter and 1 mm in thickness.

3.2. Measurements and characterization

In the present work, the CNTs are randomly dispersed in the epoxy matrix. Therefore, the dielectric permittivity ϵ is assumed to be a scalar, i.e., the samples are isotropic. The measurements of the dielectric properties of the samples were conducted using three different devices working in different frequency ranges: low frequencies from 100 mHz to 1 MHz (Solartron ModuLab XM MTS impedance analyzer), medium frequencies from 20 Hz to 120 MHz and high frequencies from 10 MHz to 18 GHz (Keysight E4990A and Agilent Technologies E8364C network analyzers, respectively).

Low frequencies measurements were conducted in free space, with the samples in contact with two electrodes. For medium and high frequency measurements, the sample is between a coaxial waveguide and a short-circuit (see in Fig. 2). The standard of the guide used is APC7mm. The thickness of the sample is around 1mm and its diameter is equal to 7mm. The complex permittivity is computed with an analytical method from the reflection coefficient measured [42]. The conductivity is then deduced:

$$\sigma_{AC} = \sigma'(\omega) = \epsilon_0 \epsilon'' \omega. \quad (30)$$

Composite samples with different CNT content were broken in liquid nitrogen and the fracture areas were observed by scanning electron microscopy (SEM, JEOL JSM-6010PLUS).

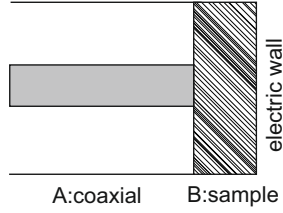


Figure 2: Geometry for medium and high frequency measurements.

4. Results and discussion

In the following computation, the length and diameter of CNT are 2 μm and 13 nm, respectively. The aspect ratio of CNT is around 150. The CNTs are assumed to be randomly dispersed in the epoxy matrix without the aggregation. The barrier height between CNT and epoxy is taken as $\Phi_0 = 30$ eV. It should be noted that the value of barrier height is identified from the AC conductivity at extremely low frequency of the CNT/epoxy nanocomposites with various CNT volume fraction. Thus it is taken as a fitting parameter rather than a physical parameter, which is different from the values presented in [22, 43]. For instance, the barrier height for epoxy is taken as 0.5-2.5 eV in [22], and the work function of CNT is considered as 5 eV in [43]. It can be seen that the different definitions of the parameters in the tunneling effect equations lead to different choices of the values. The electric and dielectric constants for CNT and epoxy are shown in Table. 1 in details. It should be noted that the dielectric constants of the components is dependent on frequency [44], which is identified from the experiment results combining with the numerical model in the present research. For instance, the real part of the dielectric permittivity of epoxy matrix is assumed as:

$$\epsilon'_m(\omega) = \begin{cases} 10 & f \leq 10 \text{ Hz}, \\ 50.25\omega^{-0.44} + 1.89 & 10 \text{ Hz} < f < 10^5 \text{ Hz}, \\ 2 & f \geq 10^5 \text{ Hz}. \end{cases} \quad (31)$$

Table 1: Electrical conductivity and dielectric permittivity of CNT and epoxy

		CNT	Epoxy	
			No tunneling	Tunneling
Dielectric permittivity	Real	$(\epsilon_c^0)' = \begin{cases} 420\omega^{-0.2}/\epsilon_0, f \leq 10 \text{ Hz} \\ (\epsilon_c^0)''/1000, f > 10 \text{ Hz} \end{cases}$	$\epsilon_m'(\omega)$	$\epsilon_t' = \epsilon_m'(\omega)\mathbf{I}$
	Imaginary	$(\epsilon_c^0)'' = \frac{\sigma_c^0}{\omega\epsilon_0}$	$\epsilon_m'' = 0.1$	$\epsilon_t'' = \frac{\sigma_t}{\omega\epsilon_0}$
Electric conductivity (S/m)		$\sigma_c^0 = 10^6$	$\sigma_m = 10^{-10}$	see σ_t in Eq. (15)

4.1. Morphology of CNT/epoxy composites

Figure 3 shows the morphology of the CNT/epoxy nanocomposites by SEM for CNT content from 0.03 vol% to 0.50 vol%. It can be seen that CNT clusters remain in the epoxy matrix. Due to the Van der Waals forces existing between CNTs, they tend to naturally form aggregates. They are about $2 \mu\text{m}$ large and decrease in size at higher CNT content (0.50 vol%) for which the dispersion is more homogeneous.

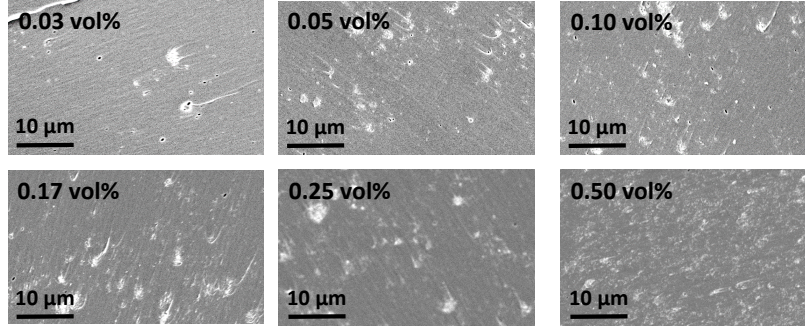


Figure 3: Morphology characterization by SEM for the nanocomposites with CNT ranging from 0.03 vol% to 0.50 vol%.

4.2. Electric conductivities of CNT/epoxy composites

Fig. 4 shows the electric conductivity of CNT/epoxy nanocomposites as a function of CNT content at the frequency of 10 Hz. Both the experimental data and the numerical results are presented, and 10 random realizations are computed for each CNT content by numerical simulation. It is obvious that the electric conductivity increases with the CNT volume percentage, and the percolation threshold is about 0.17 vol% where a dramatic increase in the electric conductivity is observed at low frequency suggesting the formation of tunneling conductive network. Below percolation threshold, the current path

can not be formed due to the low CNT content. Above percolation threshold, the CNT volume fraction is high enough to form the tunneling electric network in all the random realizations. However, it should be noted that around percolation threshold, the calculated effective electric conductivities of the realizations exhibit a distinct dispersion, ranging from 10^{-9} S/m to 10^{-5} S/m. That is to say, the electric network can only be formed by CNTs in partial realizations when the CNT content is around percolation threshold due to the specific distribution of CNTs, while the other realizations remain insulating. According to the empirical expression (see in Eq. (32)) for the prediction of the percolation threshold (ϕ_c) given by Hu et al. [45], the estimated percolation threshold for our case is about 0.4 vol%, which is higher than our data but in the same order of magnitude. The difference may result from the various processing conditions, which have strong effect on the value of percolation threshold.

$$\phi_c = (l/D)^{-1.1} \quad (32)$$

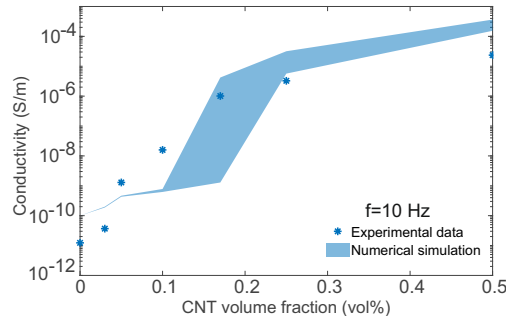


Figure 4: Experimental measurements and numerical simulation results of the AC conductivity of the CNT/epoxy nanocomposites as a function of CNT volume fractions at $f = 10$ Hz. 10 random realizations are computed for each CNT content by numerical simulation.

Fig. 5 shows the variation of electric conductivity as a function of the frequency for neat epoxy and the nanocomposites containing various CNT contents, and the experimental results are denoted by marks. For pure epoxy and the composites below the percolation threshold, the electric conductivity is frequency-dependent and increases linearly with increasing frequency in log-log scale. Beyond the percolation threshold, the CNT/polymer nanocomposite appears to be frequency-independent at low frequencies below 10^4 Hz, following by a region of linearly increasing conductivity along with the conductivity and the frequency in logarithmic scale.

The corresponding numerical estimations are presented in Fig. 5 as comparison, where 10 random realizations are computed for each CNT content. Below percolation threshold, each curve is computed by taking the average value of the samples due to their extremely small deviation, and the color region represents the interval of these samples for the nanocomposites with high CNT volume fraction above percolation threshold. It can be seen that around percolation threshold (0.17 vol%), the electric conductivities of the realizations present an enormous deviation at low frequency. The numerical results have a good agreement with the obtained experimental data for the composites beyond percolation threshold. As for the pure epoxy and the composites with 0.03 vol% CNT, the estimated electric conductivities are higher than the experimental measurements at low frequency range below 10^3 Hz. It is because that the electric conductivity of the pure epoxy has been assumed to be 10^{-10} S/m, which is 10^3 higher than the real value due to the computational limitations. It is known that the electric conductivity of epoxy is lower than 10^{-13} S/m. However, due to the computational limitations, the contrast of conductivities between CNT and polymer matrix cannot be higher than 10^{16} . Therefore, we take the electric conductivity of epoxy as 10^{-10} S/m. It has been verified that this assumption does not have any influence on the electric conductivity of the composites whose CNT content is beyond percolation threshold according to the formation of current paths by highly conductive CNTs. However, with extremely low CNT volume fraction, the epoxy matrix plays important role in the effective electric conductivity at low frequency, leading to the small disagreement between numerical estimations and experimental data.

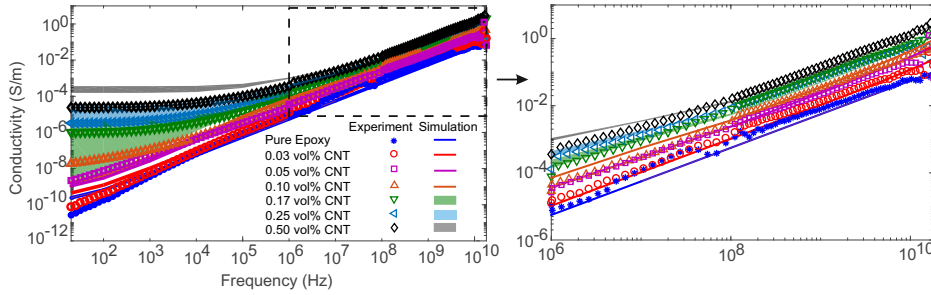


Figure 5: AC conductivity versus frequency for the CNT/epoxy nanocomposites under various CNT volume fractions. 10 random realizations are computed for each CNT content by numerical simulation.

4.3. Dielectric properties of CNT/epoxy composites

Fig. 6 depicts the frequency dependence of the real part of dielectric permittivity (ϵ') for the nanocomposites at a series of CNT content, low and high frequency range, respectively. At extremely low filler content (0.03 vol% CNT), the addition of CNTs does not change the dielectric permittivity of neat epoxy. As the CNT content increases, the real part of the dielectric permittivity of the composite grows, and exhibits a frequency-dependent behavior. It is worth noting that ϵ' decreases sharply in the low frequency range until it reaches a critical frequency, after which it remained approximately stable. The simulation results obtained using the proposed model are plotted in Fig. 6, and the interval of 10 random samples for the nanocomposite with each CNT content is represented by various color region. The deviation of ϵ' is obviously high below 100 Hz for the composites whose CNT volume fraction is beyond percolation threshold. Compared with Fig. 5, it can be supposed that the deviation of dielectric permittivity of the nanocomposites is related to the deviation of electric conductivity. It can be seen that the numerical estimations fit with the experimental results very well around the percolation threshold; for the composites with low and high CNT content, a good agreement can also be observed after 100 Hz. At high frequency range (>1 GHz), the simulation results of ϵ' have the same magnitude and the same order with the experimental measurements, although performing to be a little higher.

Fig. 7 shows the dependence of the imaginary part of dielectric permittivity (ϵ'') of the CNT/epoxy nanocomposites on frequency, which has similar characteristics as ϵ' . The increase of ϵ'' with the increasing CNT content in the nanocomposite is observed. It can be seen that for the composites whose CNT content is over 0.10 vol%, ϵ'' decreases by several orders of magnitude from 10 Hz to 10^6 Hz as shown in Fig. 7 (a), and remained unchanged at high frequency range which can be seen in Fig. 7 (b). The numerical results can reproduce the experimental dielectric behavior of the CNT/epoxy nanocomposites whose CNT volume fraction is beyond 0.10 vol%. The deviation of the results increases around percolation threshold. However, it should also be noted that for the composites with CNT content below 0.10 vol%, the numerical estimations only agree with the experiment results when the frequency is over 10^3 Hz, and show small differences at low frequency range.

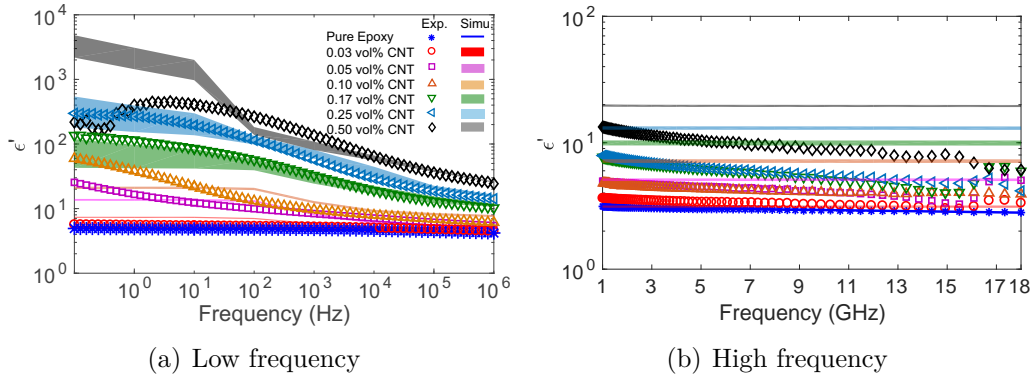


Figure 6: Real part of the relative permittivity as a function of frequency for a series of CNT/epoxy nanocomposites with different CNT volume fractions. 10 random realizations are computed for each CNT content by numerical simulation.

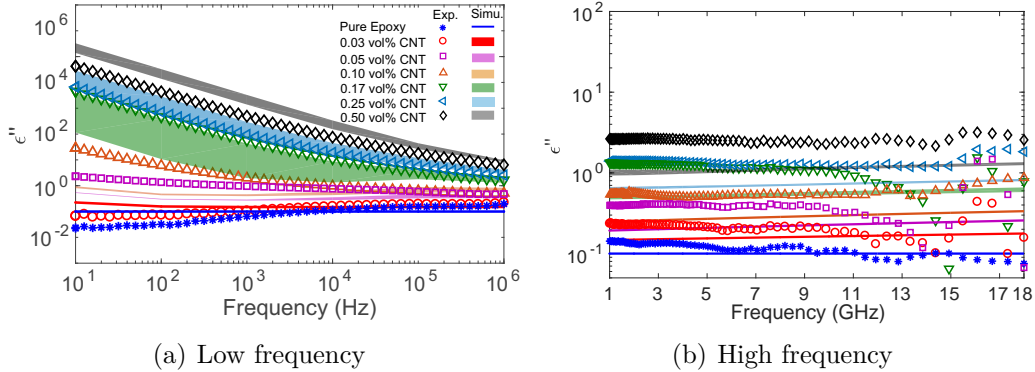


Figure 7: Imaginary part of the relative permittivity as a function of frequency for a series of CNT/epoxy nanocomposites with different CNT volume fractions. 10 random realizations are computed for each CNT content by numerical simulation.

4.4. The effect of CNT aspect ratio on AC conductivity and dielectric permittivity of nanocomposites

In this section, the effect of CNTs aspect ratio on the effective AC conductivity and dielectric permittivity is further studied by extending our calculations to the composites with various CNT aspect ratio ranging from 67 to 150. The CNT volume fraction is fixed at 0.05 vol%, and its aspect ratio is altered by changing the diameter D . In Fig. 8, the AC conductivity is computed as a function of frequency for different aspect ratio $l/D = 67, 100$ and 150 respectively. The corresponding dielectric permittivities versus

frequency are presented in Fig. 9. For each case, the interval of 10 random samples is presented by color region. It can be seen that the higher CNT aspect ratio results in larger electric conductivity and dielectric permittivity at the same frequency. The reason is that under the same CNT content, the increase of CNT aspect ratio leads to larger number of CNTs, which thus increase the local tunneling regions at the state of random distribution.

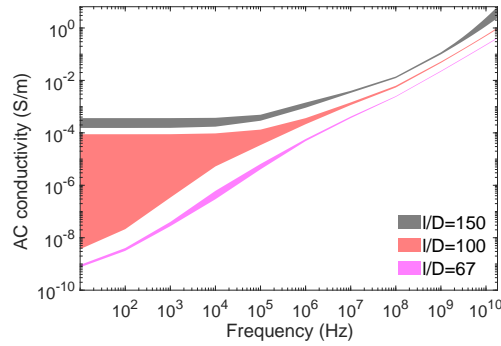


Figure 8: AC conductivity versus frequency for the CNT/epoxy nanocomposites with various CNT aspect ratio ranging from 67 to 150. The content of CNT in the composite is 0.05 vol%, $\Phi_0 = 30$ eV. 10 random realizations are computed for each CNT content by numerical simulation.

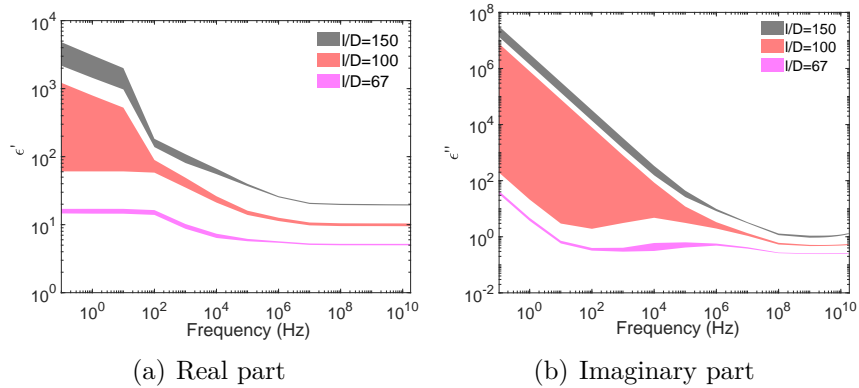


Figure 9: Relative permittivity as a function of frequency for CNT/epoxy nanocomposites with various CNT aspect ratio ranging from 67 to 150. The content of CNT in the composite is 0.05 vol%, $\Phi_0=30$ eV. 10 random realizations are computed for each CNT content by numerical simulation.

5. Conclusion

This paper presents a multiscale numerical model, developed by the authors, focusing on the prediction of the electric conductivity and dielectric permittivity of CNT/polymer nanocomposites. The tunneling effect is taken into account, which dominates the electric conductivity of the nanocomposites at low frequency. The formulations are solved by finite element method, in which the CNTs are modeled by highly conductive line segments in order to avoid meshing the extremely thin cylinders. Experimental measurements are employed by network analyzers for the AC conductivity and dielectric permittivity of CNT/epoxy nanocomposites under a wide frequency range. The dielectric properties of the components in the composites are identified by combining both the numerical model and the experiment results. It is shown that the dielectric permittivities of CNT and epoxy matrix are frequency-dependent. The simulation results are compared to the experimental results on CNT/epoxy nanocomposite, showing a good agreement in the electric conductivity, as well as in the dielectric permittivity for the composites whose CNT content is above percolation threshold. Below percolation threshold, the numerical model works well when the frequency is over 10^3 Hz. Furthermore, the effects of CNT aspect ratio are simulated with this technique, showing that the higher CNT aspect ratio results in larger AC conductivity and permittivity of the composites at the same frequency.

6. Acknowledgements

This work has benefited from the financial support of the LabEx LaSIPS (ANR-10-LABX-0032-LaSIPS) managed by the French National Research Agency under the “Investissements d’avenir” program (ANR-11-IDEX-0003).

References

- [1] M. Rahmat, P. Hubert, Carbon nanotube–polymer interactions in nanocomposites: a review, *Composites Science and Technology* 72 (1) (2011) 72–84.
- [2] O. Breuer, U. Sundararaj, Big returns from small fibers: a review of polymer/carbon nanotube composites, *Polymer Composites* 25 (6) (2004) 630–645.

- [3] N. Li, Y. Huang, F. Du, X. He, X. Lin, H. Gao, Y. Ma, F. Li, Y. Chen, P. C. Eklund, Electromagnetic interference (emi) shielding of single-walled carbon nanotube epoxy composites, *Nano letters* 6 (6) (2006) 1141–1145.
- [4] M. H. Al-Saleh, U. Sundararaj, Electromagnetic interference shielding mechanisms of cnt/polymer composites, *Carbon* 47 (7) (2009) 1738–1746.
- [5] T. Chen, L. Dai, Carbon nanomaterials for high-performance supercapacitors, *Materials Today* 16 (7-8) (2013) 272–280.
- [6] I. M. De Rosa, F. Sarasini, M. S. Sarto, A. Tamburrano, Emc impact of advanced carbon fiber/carbon nanotube reinforced composites for next-generation aerospace applications, *IEEE transactions on Electromagnetic Compatibility* 50 (3) (2008) 556–563.
- [7] A. Fletcher, M. C. Gupta, K. L. Dudley, E. Vedeler, Elastomer foam nanocomposites for electromagnetic dissipation and shielding applications, *Composites Science and Technology* 70 (6) (2010) 953–958.
- [8] S. C. Tjong, G. Liang, S. Bao, Electrical behavior of polypropylene/multiwalled carbon nanotube nanocomposites with low percolation threshold, *Scripta Materialia* 57 (6) (2007) 461–464.
- [9] C. Han, A. Gu, G. Liang, L. Yuan, Carbon nanotubes/cyanate ester composites with low percolation threshold, high dielectric constant and outstanding thermal property, *Composites Part A: Applied Science and Manufacturing* 41 (9) (2010) 1321–1328.
- [10] J.-K. Yuan, S.-H. Yao, Z.-M. Dang, A. Sylvestre, M. Genestoux, J. Bail, Giant dielectric permittivity nanocomposites: realizing true potential of pristine carbon nanotubes in polyvinylidene fluoride matrix through an enhanced interfacial interaction, *The Journal of Physical Chemistry C* 115 (13) (2011) 5515–5521.
- [11] M. Jomaa, K. Masenelli-Varlot, L. Seveyrat, L. Lebrun, M. D. Jawhar, E. Beyou, J.-Y. Cavallé, Investigation of elastic, electrical and electromechanical properties of polyurethane/grafted carbon nanotubes nanocomposites, *Composites Science and Technology* 121 (2015) 1–8.

- [12] Z.-M. Dang, L. Wang, Y. Yin, Q. Zhang, Q.-Q. Lei, Giant dielectric permittivities in functionalized carbon-nanotube/electroactive-polymer nanocomposites, *Advanced Materials* 19 (6) (2007) 852–857.
- [13] Q. Li, Q. Xue, L. Hao, X. Gao, Q. Zheng, Large dielectric constant of the chemically functionalized carbon nanotube/polymer composites, *Composites Science and Technology* 68 (10-11) (2008) 2290–2296.
- [14] S. Begum, H. Ullah, A. Kausar, M. Siddiq, M. A. Aleem, Fabrication of epoxy functionalized mwcnts reinforced pvdf nanocomposites with high dielectric permittivity, low dielectric loss and high electrical conductivity, *Composites Science and Technology* 167 (2018) 497–506.
- [15] J. Chang, G. Liang, A. Gu, S. Cai, L. Yuan, The production of carbon nanotube/epoxy composites with a very high dielectric constant and low dielectric loss by microwave curing, *Carbon* 50 (2) (2012) 689–698.
- [16] X. Zhang, G. Liang, J. Chang, A. Gu, L. Yuan, W. Zhang, The origin of the electric and dielectric behavior of expanded graphite–carbon nanotube/cyanate ester composites with very high dielectric constant and low dielectric loss, *Carbon* 50 (14) (2012) 4995–5007.
- [17] A. Ameli, M. Nofar, C. Park, P. Pötschke, G. Rizvi, Polypropylene/carbon nanotube nano/microcellular structures with high dielectric permittivity, low dielectric loss, and low percolation threshold, *Carbon* 71 (2014) 206–217.
- [18] X. Huang, P. Jiang, C. Kim, F. Liu, Y. Yin, Influence of aspect ratio of carbon nanotubes on crystalline phases and dielectric properties of poly (vinylidene fluoride), *European Polymer Journal* 45 (2) (2009) 377–386.
- [19] A. Sihvola, Mixing rules with complex dielectric coefficients, *Subsurface sensing technologies and applications* 1 (4) (2000) 393–415.
- [20] P. Kuzhir, A. Paddubskaya, D. Bychanok, A. Nemilentsau, M. Shuba, A. Plusch, S. Maksimenko, S. Bellucci, L. Coderoni, F. Micciulla, et al., Microwave probing of nanocarbon based epoxy resin composite films: Toward electromagnetic shielding, *Thin Solid Films* 519 (12) (2011) 4114–4118.

- [21] L. L. Vovchenko, O. V. Lozitsky, L. Y. Matsui, O. S. Yakovenko, V. V. Oliynyk, V. V. Zagorodnii, Modeling of dielectric permittivity of polymer composites with mixed fillers, in: International Conference on Nanotechnology and Nanomaterials, Springer, 2018, pp. 349–365.
- [22] N. Hu, Y. Karube, M. Arai, T. Watanabe, C. Yan, Y. Li, Y. Liu, H. Fukunaga, Investigation on sensitivity of a polymer/carbon nanotube composite strain sensor, *Carbon* 48 (3) (2010) 680–687.
- [23] L. Y. Alamusu, N. Hu, Numerical simulations on piezoresistivity of cnt/polymer based nanocomposites, *Computers Materials & Continua* 20 (2010) 101–117.
- [24] X. Xia, Y. Wang, Z. Zhong, G. J. Weng, A frequency-dependent theory of electrical conductivity and dielectric permittivity for graphene-polymer nanocomposites, *Carbon* 111 (2017) 221–230.
- [25] X. Zhao, Y. Wu, Z. Fan, F. Li, Three-dimensional simulations of the complex dielectric properties of random composites by finite element method, *Journal of Applied Physics* 95 (12) (2004) 8110–8117.
- [26] Y. Cheng, X. Chen, K. Wu, S. Wu, Y. Chen, Y. Meng, Modeling and simulation for effective permittivity of two-phase disordered composites, *Journal of Applied Physics* 103 (3) (2008) 034111.
- [27] R. Simoes, J. Silva, R. Vaia, V. Sencadas, P. Costa, J. Gomes, S. Lanceros-Méndez, Low percolation transitions in carbon nanotube networks dispersed in a polymer matrix: dielectric properties, simulations and experiments, *Nanotechnology* 20 (3) (2008) 035703.
- [28] Z. Wang, J. K. Nelson, H. Hillborg, S. Zhao, L. S. Schadler, Dielectric constant and breakdown strength of polymer composites with high aspect ratio fillers studied by finite element models, *Composites Science and Technology* 76 (2013) 29–36.
- [29] B. Widom, Random sequential addition of hard spheres to a volume, *The Journal of Chemical Physics* 44 (10) (1966) 3888–3894.
- [30] N. Hu, Y. Karube, C. Yan, Z. Masuda, H. Fukunaga, Tunneling effect in a polymer/carbon nanotube nanocomposite strain sensor, *Acta Materialia* 56 (13) (2008) 2929–2936.

- [31] C. Geuzaine, J.-F. Remacle, Gmsh: A 3-d finite element mesh generator with built-in pre-and post-processing facilities, *International journal for numerical methods in engineering* 79 (11) (2009) 1309–1331.
- [32] X. Lu, J. Yvonnet, F. Detrez, J. Bai, Multiscale modeling of nonlinear electric conductivity in graphene-reinforced nanocomposites taking into account tunnelling effect, *Journal of Computational Physics* 337 (2017) 116–131.
- [33] X. Lu, J. Yvonnet, F. Detrez, J. Bai, Low electrical percolation thresholds and nonlinear effects in graphene-reinforced nanocomposites: a numerical analysis, *Journal of Composite Materials* 52 (20) (2018) 2767–2775.
- [34] X. Lu, F. Detrez, J. Yvonnet, J. Bai, Multiscale study of influence of interfacial decohesion on piezoresistivity of graphene/polymer nanocomposites, *Modelling and Simulation in Materials Science and Engineering* 27 (3) (2019) 035001.
- [35] J. G. Simmons, Generalized formula for the electric tunnel effect between similar electrodes separated by a thin insulating film, *Journal of Applied Physics* 34 (6) (1963) 1793–1803.
- [36] T. Hertel, R. E. Walkup, P. Avouris, Deformation of carbon nanotubes by surface van der waals forces, *Physical Review B* 58 (20) (1998) 13870.
- [37] L. Girifalco, M. Hodak, R. S. Lee, Carbon nanotubes, buckyballs, ropes, and a universal graphitic potential, *Physical Review B* 62 (19) (2000) 13104.
- [38] A. Bossavit, "small parameter" problems in eddy-current theory: a review, and case-study on how to avoid meshing small air-gaps, *IEEE transactions on Magnetics* 32 (3) (1996) 729–732.
- [39] S. Gu, Q.-C. He, Interfacial discontinuity relations for coupled multifield phenomena and their application to the modeling of thin interphases as imperfect interfaces, *Journal of the Mechanics and Physics of Solids* 59 (7) (2011) 1413–1426.
- [40] J. Yvonnet, Q.-C. He, C. Toulemonde, Numerical modelling of the effective conductivities of composites with arbitrarily shaped inclusions and

- highly conducting interface, *Composites Science and Technology* 68 (13) (2008) 2818–2825.
- [41] D. He, B. Fan, H. Zhao, M. Yang, H. Wang, J. Bai, W. Li, X. Zhou, J. Bai, Multifunctional polymer composites reinforced by carbon nanotubes–alumina hybrids with urchin-like structure, *Materials Today Communications* 11 (2017) 94–102.
- [42] N.-E. Belhadj-Tahar, A. Fourrier-Lamer, Broad-band analysis of a coaxial discontinuity used for dielectric measurements, *IEEE transactions on Microwave Theory and Techniques* 34 (3) (1986) 346–350.
- [43] C. Li, E. T. Thostenson, T.-W. Chou, Dominant role of tunneling resistance in the electrical conductivity of carbon nanotube–based composites, *Applied Physics Letters* 91 (22) (2007) 223114.
- [44] A. K. Jonscher, The ‘universal’ dielectric response, *Nature* 267 (5613) (1977) 673.
- [45] N. Hu, Z. Masuda, C. Yan, G. Yamamoto, H. Fukunaga, T. Hashida, The electrical properties of polymer nanocomposites with carbon nanotube fillers, *Nanotechnology* 19 (21) (2008) 215701.